ISSN 0031-918X, Physics of Metals and Metallography, 2019, Vol. 120, No. 6, pp. 614–619. © Pleiades Publishing, Ltd., 2019.
Russian Text © The Author(s), 2019, published in Fizika Metallov i Metallovedenie, 2019, Vol. 120, No. 6, pp. 668–672.

## STRENGTH AND PLASTICITY

# Evolution of Microstructure and Mechanical Properties of a New Al–Cu–Er Wrought Alloy

**A. V. Pozdnyakov[a], *, R. Yu. Barkov[a], Zh. Sarsenbaev[a], S. M. Amer[a], and A. S. Prosviryakov[a]**

[a] *National University of Science and Technology MISiS, Moscow, 119049 Russia*

**e-mail: pozdniakov@misis.ru*

Received November 27, 2018; revised December 18, 2018; accepted December 29, 2018

**Abstract**—The evolution of the microstructure and mechanical properties of deformed sheets made of a new Al–4Cu–2.7Er alloy has been studied in the course of homogenization and annealing. The structure of the cast alloy consists of a dispersed eutectic ((Al) + $Al_8Cu_4Er$), $Al_3Er$-phase inclusions located along the dendritic-cell boundaries, and a nonequilibrium AlCu phase. During annealing at 605°C before quenching, the intermetallic phases have high thermal stability: the particle size of $Al_8Cu_4Er$ and $Al_3Er$ phases does not exceed 1–4 μm. The annealing of deformed sheets at temperatures below 300°C leads to a slight decrease in the hardness; grains elongated along the rolling direction are observed in the structure. With an increase in the annealing temperature from 350 to 550°C, the recrystallized grain size increases from 8 ± 1 to 14.5 ± 1.5 μm. The uniaxial tensile tests showed that the annealed alloy possesses sufficiently high strength characteristics: yield stress of 260–280 MPa, ultimate tensile strength of 291–312 MPa, and relative elongation of 5.5–6.1%.

*Keywords:* aluminum alloys, rare-earth metals, erbium, microstructure, heat treatment, hardness

**DOI:** 10.1134/S0031918X19060097

## INTRODUCTION

The Al–Cu alloys are characterized by high strength at room and high temperatures, but possess the lowest casting properties among all aluminum alloys [1–5]. The casting characteristics of these alloys can be increased by the introduction of eutectic-forming additives, such as Si, Ni, Fe, and Mn; however, in this case, their plasticity can significantly decrease [5, 6]. On the other hand, the search for new alloying systems for aluminum–copper alloys is of great interest. For example, the authors of [7–9] showed that in the alloys with compositions that lie on the quasibinary sections of the Al–Cu–Ce [7, 8] and Al–Cu–Y systems [9], there are almost no crystallization cracks because of a narrow crystallization range. In this case, the arising eutectic $Al_8Cu_4Ce$ [7, 8] and $Al_8Cu_4Y$ [9] phases differ in high dispersion and thermal stability at homogenization temperatures above 590°C. The quasibinary Al–$Al_8Cu_4Er$ alloys in the Al–Cu–Er system also have a narrow crystallization range [10, 11] and may be of interest for developing new materials based on them. It should be noted that the addition of small amounts of erbium to aluminum and Al–Mg alloys contributes to the refinement of grain and to strengthening during annealing, especially in the presence of zirconium [12–22].

This work is aimed at the study of the evolution of the structure and mechanical properties of the quasibinary Al–4Cu–2.7Er alloy during homogenization and annealing of deformed sheets.

## EXPERIMENTAL

The Al–4Cu–2.7Er alloy was melted from aluminum of grade A99 [23] and Al–53.5% Cu and Al–9% Er master alloys using a resistance furnace. The temperature of melting and casting was 750°C. The melt was cast into a copper water-cooled mold with an inner size of 20 × 40 × 120 mm. The ingot after heat treatment was rolled to a thickness of 10 mm at a temperature of 440°C and to 1 mm at room temperature. The heat treatment was carried out using Nabertherm and SNOL drying cabinets with an accuracy of maintaining the temperature of 1 K.

The samples for microstructural studies were prepared using a Struers Labopol-5 grinding/polishing machine. The microstructural studies and phase identification were performed using a Neophot-30 optical microscope, a TESCAN VEGA 3LMH scanning electron microscope (SEM) equipped with an X-Max 80 energy-dispersive spectroscopy attachment, and a Bruker D8 Advance X-ray diffractometer with a holding for 20 s at each point with a step of 0.05°. The differential scanning calorimetry (DSC) was carried out using a Labsys Setaram calorimeter.

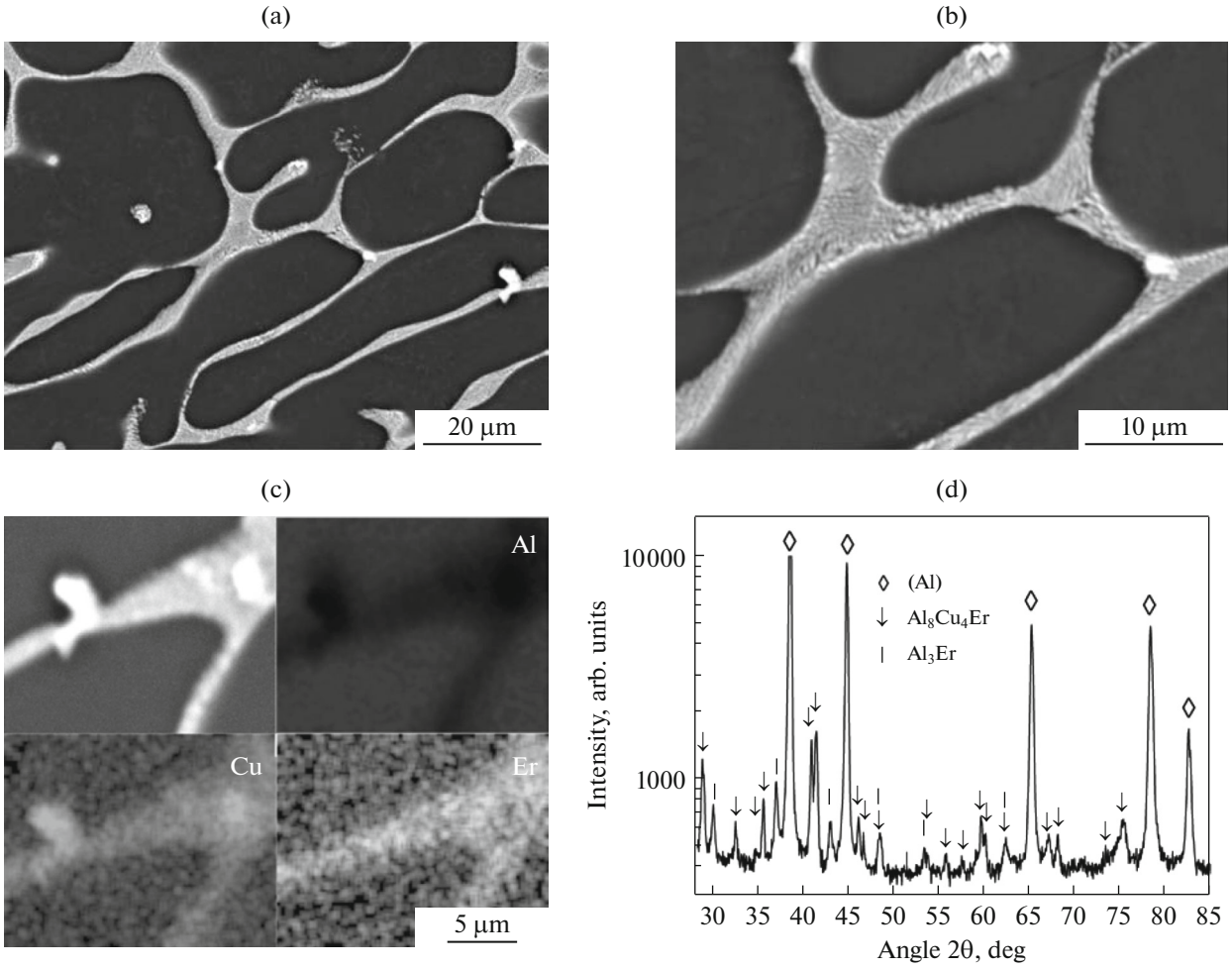


**Fig. 1.** (a, b) SEM images of the microstructure, (c) maps of the element distribution between phases, and (d) X-ray diffraction pattern of the cast Al–4Cu–2.7Er alloy.

The Vickers hardness was measured under a load $F = 49$ N (5 kgf). The determination error did not exceed 3 HV. The tests were carried out using a Zwick/Roll Z250 Series Allround universal testing machine with an automatic sensor for longitudinal deformation.

## RESULTS AND DISCUSSION

Figure 1 shows (a, b) the microstructures of the cast alloy and (c, d) the results of the investigation of the phase composition: (c) of the distribution of elements between the phases and (d) of the X-ray diffraction analysis. The structure represents a dispersed eutectic with a thickness of the second phase of less than 200 nm. A brighter dispersed phase with the same size precipitates at the boundaries of the dendrite cells. Coarser bright inclusions with a size of about 1 μm also occur. These inclusions, as it follows from the distribution of the elements between the phases, are enriched in copper (Fig. 1c). According to the EDS analysis, their composition corresponds to the AlCu phase. However, the X-ray diffraction pattern (Fig. 1d) contains peaks belonging to aluminum and the $Al_3Er$ and $Al_8Cu_4Er$ phases.

The AlCu phase apparently is nonequilibrium. Since its amount is small, it was not possible to identify it using X-ray diffraction analysis. Thus, it can be said that the structure is represented by a dispersed eutectic ((Al) + $Al_8Cu_4Er$), $Al_3Er$-phase inclusions located along the dendritic cell boundaries, and an nonequilibrium AlCu phase. Figure 2 shows the result of the calorimetric analysis (DSC curves). In the heating curve (lower curve), no peaks of the nonequilibrium AlCu phase were revealed, which may be caused by its small amount; the phase is dissolved during heating. The solidus temperature was 613°C. During heating, the eutectic ((Al) + Al8Cu4Er) begins to dissolve at the melting point. This corresponds to the first peak in the lower curve. The second peak corresponds to the melting of primary aluminum crystals. The peak

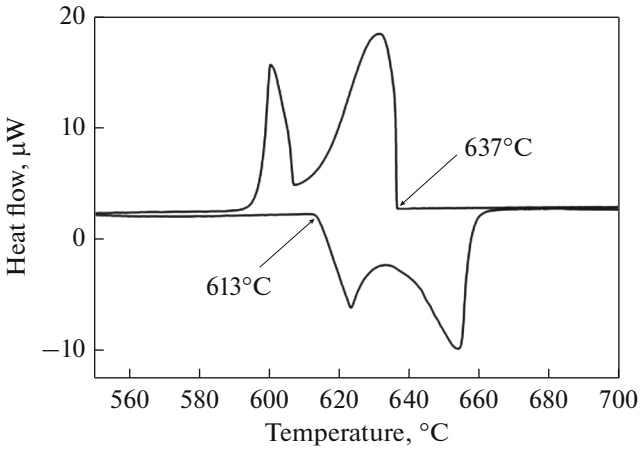


**Fig. 2.** DSC curve of the Al–4Cu–2.7Er alloy. The lower line is the heating curve; the upper, the cooling curve.

corresponding to the dissolution of the $Al_3Er$ phase is overlapped by two large peaks corresponding to the melting of the eutectic and primary crystals. The liquidus temperature of the alloy was 637°C (the upper curve in Fig. 2).

In accordance with the determined solidus temperature, the homogenization of the alloy was carried out by annealing at the temperature of 605°C for 1, 3, 6, and 24 h. Figure 3 shows the corresponding microstructures of the annealed samples. The copper content in the aluminum solid solution in the ingot is 1.8 wt %. After a 1-h annealing, it increases to 2.2 wt % and remains unchanged with increasing annealing time. This growth is apparently caused by the dissolution of the nonequilibrium AlCu phase. During annealing, the fragmentation and spheroidization of the $Al_3Er$ and $Al_8Cu_4Er$ phases occur. These intermetallic phases possess high thermal stability. After annealing for one hour, their size is 1–4 μm (Fig. 3a), which remains virtually unchanged with an increase in the annealing time to 24 h (Figs. 3b–3d). However, the fraction of particles with a size of less than 2 μm is significantly higher.

Before rolling, the alloy ingot was quenched from 605°C after holding for 1 h. After rolling, the sheet was annealed for 1 h at temperatures in the 100–550°C range. During annealing at temperatures of up to 300°C, the hardness decreases from 100 HV (deformed state) to 70 HV, while the structure remains

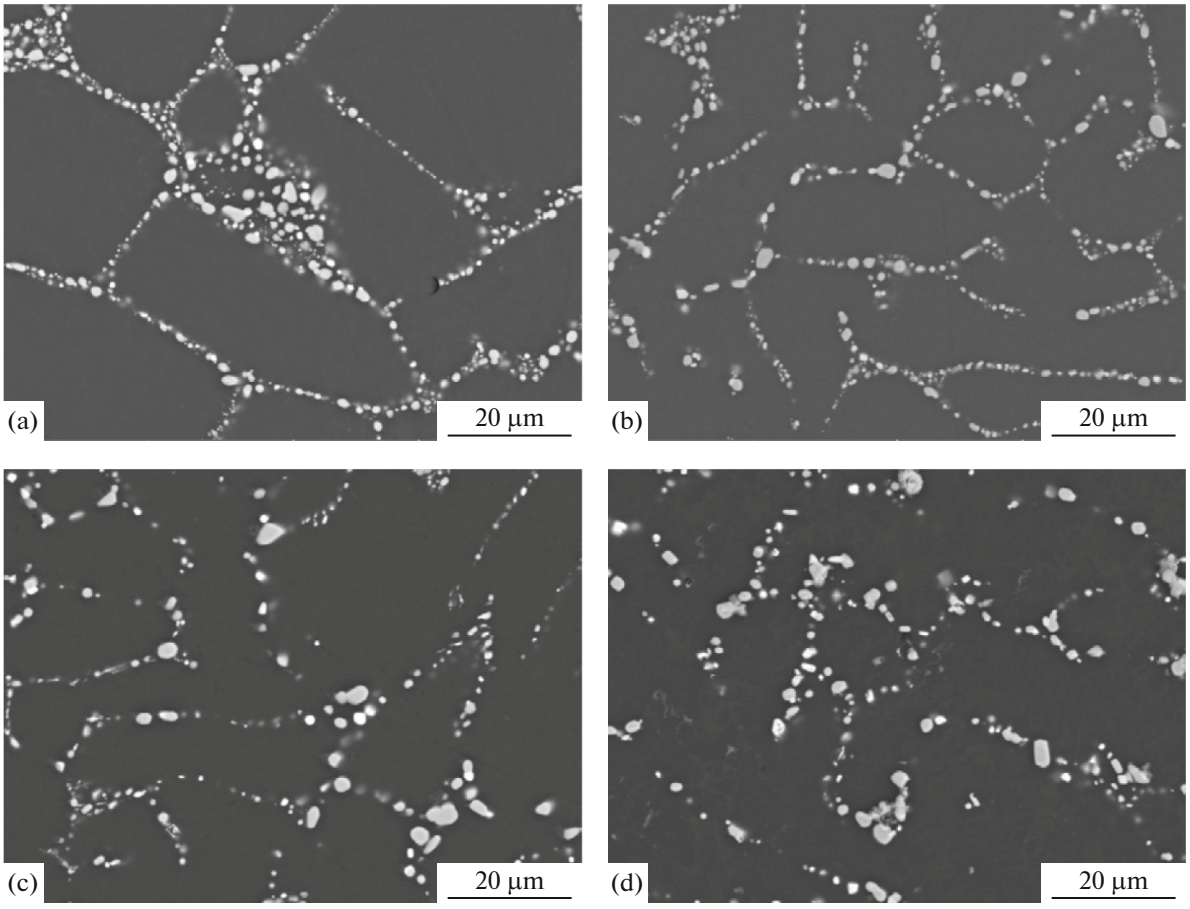


**Fig. 3.** Evolution of the microstructure of the alloy during annealing at 605°C for (a) 1, (b) 3, (c) 6, and (d) 24 h.

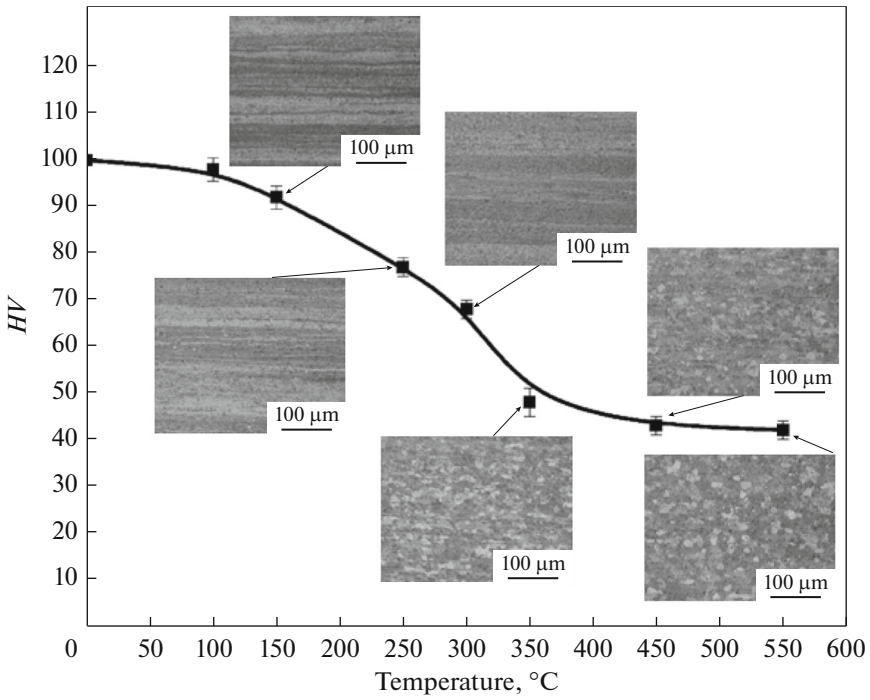


**Fig. 4.** Dependence of the hardness on the temperature of annealing for 1 h.

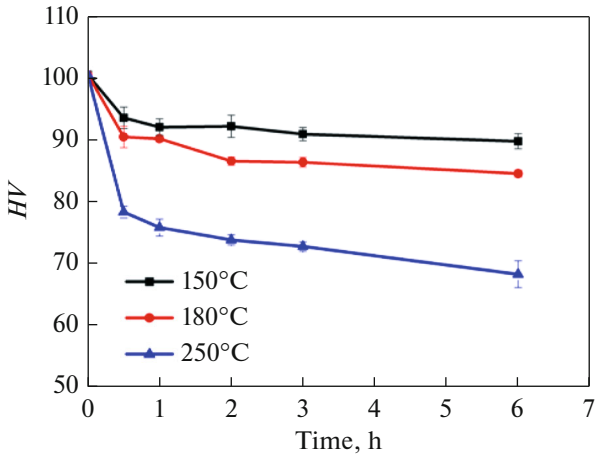


**Fig. 5.** Dependence of the hardness on the time of annealing at 150, 180, and 250°C.

nonrecrystallized (Fig. 4). The softening is caused by the processes of polygonization. The annealing at above 350°C for 1 h leads to a recrystallization. In this case, an increase in the annealing temperature from 350 to 550°C leads to an increase in the recrystallized grain size from 8±1 to 14.5±1.5 μm. It is known that the coarse particles with a size of 1–2 μm stimulate nucleation upon recrystallization owing to the appearance of deformation-induced lattice distortions near such particles [24–27]. With an increase in the annealing time to 6 h at low temperatures of 150 and 180°C, the hardness decreases insignificantly and is 90 and 85 HV, respectively (Fig. 5).

The uniaxial tensile tests showed that the annealed alloy has sufficiently high strength characteristics: yield stress of 260–280 MPa, ultimate tensile strength of 291–312 MPa, and relative elongation of 5.5–6.1% (Table 1). For comparison, the Al–Cu–Y alloy of similar composition has the following properties: $\sigma_{0.2}$ =

**Table 1.** Mechanical tensile properties of the Al–4Cu–2.7Er alloy in the deformed and annealed states

| State | $\sigma_{0.2}$, MPa | $\sigma_u$, MPa | $\delta$, % |
|---|---|---|---|
| Deformed | 285 ± 3 | 318 ± 1 | 4.5 ± 0.2 |
| Annealing at 100°C for 1 h | 280 ± 2 | 312 ± 2 | 5.7 ± 0.5 |
| Annealing at 100°C for 3 h | 276 ± 2 | 312 ± 1 | 6.1 ± 0.1 |
| Annealing at 150°C for 1 h | 262 ± 1 | 296 ± 2 | 5.5 ± 0.3 |
| Annealing at 150°C for 3 h | 260 ± 1 | 291 ± 2 | 5.8 ± 0.4 |
| Annealing at 250°C for 0.5 h | 220 ± 2 | 240 ± 1 | 6.0 ± 0.2 |

248–276 MPa, $\sigma_u$ = 278–310 MPa, and $\delta$ = 5.8–6.6% [9].

## CONCLUSIONS

The structure and properties of a new wrought alloy of the Al–Cu–Er system have been studied. Scanning electron microscopy and X-ray diffraction analysis have shown that the cast structure is represented by a dispersed eutectic ((Al) + $Al_8Cu_4Er$), $Al_3Er$-phase inclusions located along the dendritic cell boundaries, and AlCu nonequilibrium phase. The intermetallic phases are characterized by high thermal stability during annealing before quenching at 605°C. After homogenization, the size of the $Al_8Cu_4Er$ and $Al_3Er$ phases does not exceed 1–4 μm. Upon annealing for 1 h at temperatures above 350°C, a recrystallization occurs in the wrought alloy. With an increase in the annealing temperature from 350 to 550°C, the recrystallized grain size increases from 8 ± 1 to 14.5 ± 1.5 μm. The uniaxial tensile tests have shown that for the annealed alloy, the yield stress is 260–280 MPa, the ultimate tensile strength is 291–312 MPa, and the relative elongation is 5.5–6.1%.

## FUNDING

The work was supported by the Russian Science Foundation (project no. 17-79-10256)

## REFERENCES

1. I. I. Novikov, *Hot Brittleness of Non-Ferrous Metals and Alloys* (Nauka, Moscow, 1966) [in Russian].
2. D. G. Eskin and L. Suyitno Katgerman, "Mechanical properties in the semi-solid state and hot tearing of aluminium alloys," Prog. Mater. Sci. **49**, 629–711 (2004).
3. V. S. Zolotorevsky, N. A. Belov, and M. V. Glazoff, *Casting Aluminum Alloys* (Alcoa Technical Center, Alcoa Center, PA, 2007).
4. *ASM HANDBOOK* Vol. 2: *Properties and Selection: Nonferrous Alloys and Special-Purpose Materials* (ASM International, Metals Park, OH, 2010).
5. V. S. Zolotorevskiy and A. V. Pozdniakov, "Determining the hot cracking index of Al–Si–Cu–Mg casting alloys calculated using the effective solidification range," Int. J. Cast Met. Res. **27**, No. 4, 193–198 (2014).
6. V. S. Zolotorevskiy, A. V. Pozdniakov, and A. Yu. Churyumov, "Search for promising compositions for developing new multiphase casting alloys based on Al–Cu–Mg matrix using thermodynamic calculations and mathematic simulation," Phys. Met. Metallogr. **113**, 1052–1060 (2012).
7. N. A. Belov, A. V. Khvan, and A. N. Alabin, "Microstructure and phase composition of Al–Ce–Cu alloys in the Al-rich corner," Mater. Sci. Forum **519–521** (Part 1), 395–400 (2006).
8. N. A. Belov and A. V. Khvan, "The ternary Al–Ce–Cu phase diagram in the aluminum-rich corner," Acta Mater. **55**, 5473–5482 (2007).
9. A. V. Pozdniakov and R. Y. Barkov, "Microstructure and materials characterisation of the novel Al–Cu–Y alloy," Mater. Sci. Technol. **34**, 1489–1496 (2018).
10. L. Zhang, P. J. Masset, F. Cao, F. Meng, L. Liu, and Z. Jin, "Phase relationships in the Al-rich region of the Al–Cu–Er system," J. Alloys Compd. **509**, 3822–3831 (2011).
11. L. G. Zhang, L. B. Liu, G. X. Huang, H. Y. Qi, B. R. Jia, and Z. P. Jin, "Thermodynamic assessment of the Al–Cu–Er system," CALPHAD **32**, 527–534 (2008).
12. S. P. Wen, K. Y. Gao, Y. Li, H. Huang, and Z. R. Nie, "Synergetic effect of Er and Zr on the precipitation hardening of Al–Er–Zr alloy," Scr. Mater. **65**, 592–595 (2011).
13. S. P. Wen, K. Y. Gao, H. Huang, W. Wang, and Z. R. Nie, "Precipitation evolution in Al–Er–Zr alloys during aging at elevated temperature," J. Alloys Compd. **574**, 92–97 (2013).
14. Y. Zhang, K. Gao, S. Wen, H. Huang, Z. Nie, and D. Zhou, "The study on the coarsening process and precipitation strengthening of $Al_3Er$ precipitates in Al–Er binary alloy," J. Alloys Compd. **610**, 27–34 (2014).
15. A. V. Pozdnyakov, A. A. Osipenkova, D. A. Popov, S. V. Makhov, and V. I. Napalkov, "Effect of low additions of Y, Sm, Gd, Hf and Er on the structure and hardness of alloy Al–0.2% Zr–0.1% Sc," Met. Sci. Heat Treat. **58**, 537–542 (2017).
16. A. V. Pozdniakov, R. Y. Barkov, A. S. Prosviryakov, A. Y. Churyumov, I. S. Golovin, and V. S. Zolotorevskiy, "Effect of Zr on the microstructure, recrystallization behavior, mechanical properties and electrical conductivity of the novel Al–Er–Y alloy," J. Alloys Compd. **765**, 1–6 (2018).

17. L. Z. He, X. H. Li, X. T. Liu, X. J. Wang, H. T. Zhang, and J. Z. Cui, "Effects of homogenization on microstructures and properties of a new type Al–Mg–Mn–Zr–Ti–Er alloy," Mater. Sci. Eng., A **527**, 7510–7518 (2010).

18. H. L. Hao, D. R. Ni, Z. Zhang, D. Wang, B. L. Xiao, and Z. Y. Ma, "Microstructure and mechanical properties of Al–Mg–Er sheets jointed by friction stir welding," Mater. Des. **52**, 706–712 (2013).

19. Y. Dongxi, L. Xiaoyan, H. Dingyong, and H. Hui, "Effect of minor Er and Zr on microstructure and mechanical properties of Al–Mg–Mn alloy (5083) welded joints," Mater. Sci. Eng., A **561**, 226–231 (2013).

20. M. Song, K. Du, Z. Y. Huang, H. Huang, Z. R. Nie, and H. Q. Ye, "Deformation-induced dissolution and growth of precipitates in an Al–Mg–Er alloy during high-cycle fatigue," Acta Mater. **81**, 409–419 (2014).

21. S. P. Wen, W. Wang, W. H. Zhao, X. L. Wu, K. Y. Gao, H. Huang, and Z. R. Nie, "Precipitation hardening and recrystallization behavior of Al–Mg–Er–Zr alloys," J. Alloys Compd. **687**, 143–151 (2016).

22. A. V. Pozdniakov, V. Yarasu, R. Yu. Barkov, O. A. Yakovtseva, S. V. Makhov, and V. I. Napalkov, "Microstructure and mechanical properties of novel Al–Mg–Mn–Zr–Sc–Er alloy," Mater. Lett. **202**, 116–119 (2017).

23. *Russian State Standard GOST 11069-2001. Primary Aluminum. Grades* (Moscow, 2001) [in Russian].

24. F. J. Humphreys and M. Hatherly, *Recrystallization and Related Annealing Phenomena* (Pergamon Press, Oxford, 1995).

25. E. Nes and J. A. Wert, "Modeling of recrystallization in alloys with a bimodal particle size distribution," Scr. Metall. **18**, 1433–1438 (1984).

26. R. Ørsund and E. Nes, "A model for the nucleation of recrystallization from particles: The texture aspect," Scr. Metall. **22**, 671–676 (1988).

27. A. V. Mikhaylovskaya, M. A. Ryazantseva, and V. K. Portnoy, "Effect of eutectic particles on the grain size control and the superplasticity of aluminium alloys," Mater. Sci. Eng., A **528**, 7306–7309 (2011).

*Translated by O. Golosova*